LLNL-PRES-512837

Five-Field Peeling-Ballooning Modes Simulation and Differencing Schemes Comparison with BOUT++ Code

Tianyang Xia[1,2], Xueqiao Xu[2], Ben Dudson[3] and Jangang Li[1]

[1]Institute of Plasma Physics, Chinese Academy of Sciences, Hefei, China.
[2]Lawrence Livermore National Laboratory, Livermore, CA 94550, USA
[3]University of York, Heslington, York YO10 5DD, United Kindom

53rd Annual Meeting of the APS Division of Plasma Physics
Salt Lake City, Utah
Nov 15, 2010

This work was performed under the auspices of the U.S. Department of Energy by Lawrence Livermore National Security, LLC, Lawrence Livermore National Laboratory under Contract DE-AC52-07NA27344, and is supported by the China Natural Science Foundation under Contract No.10721505.

Introduction

➢The fast-reconnection simulation of ELMs with BOUT++ code in high-confinement mode tokamak discharges has been reported by Xu, et al. [PRL, Vol. 105, 175005 (2010)]. We have extended these initial BOUT++ simulations by adding the effects of the parallel velocity, Hall effect, parallel viscosity and hyper-diffusion in both linear and nonlinear phases [Xia, Xu, Dudson & Li, accepted by Contributions to Plasma Physics]. This is important in order to capture the impact of ion density on tokamak experiments; e.g. in EDA-H mode and I-mode on Alcator C-Mod. Here we improve the previous two-fluid simulations of the pedestal collapse by separating the pressure into ion density, ion and electron temperature equations.

➢In BOUT++ code, there are various differencing schemes, and the 3rd order WENO schemes are applied in the advection and magnetic flutter term in previous ELM simulations. In order to find the most robust scheme, we test the different combinations of schemes in the perpendicular direction. The tests for 3rd order WENO, Arakawa, CTU, upwind and central schemes will be reported here.

Background

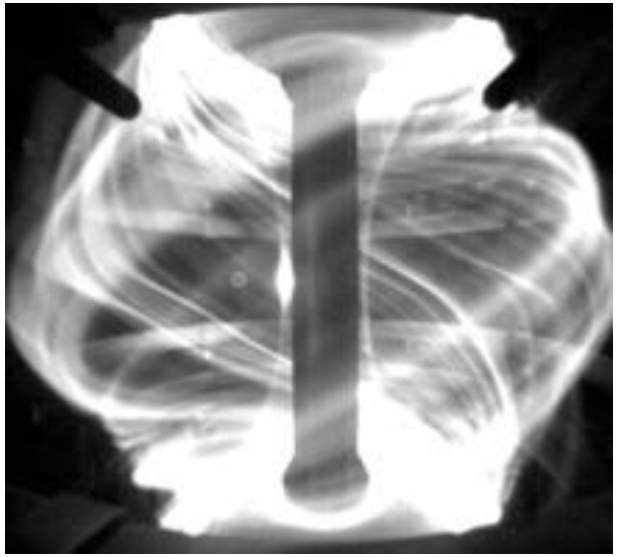

ELMs in MAST

In H-mode, the localized edge modes (ELMs) is a dangerous perturbation for large tokamaks, such as ITER. ELMs are triggered by ideal MHD instabilities. The type I ELM is successfully explained by ideal peeling-ballooning (P-B) theory in pedestal, in which the steep pressure gradients drive ballooning mode and bootstrap current generates peeling mode.

BOUT++ simulates the Peeling-Ballooning modes through two fluid framework, which could study the nonlinear dynamics of ELMs including extensions beyond MHD physics.

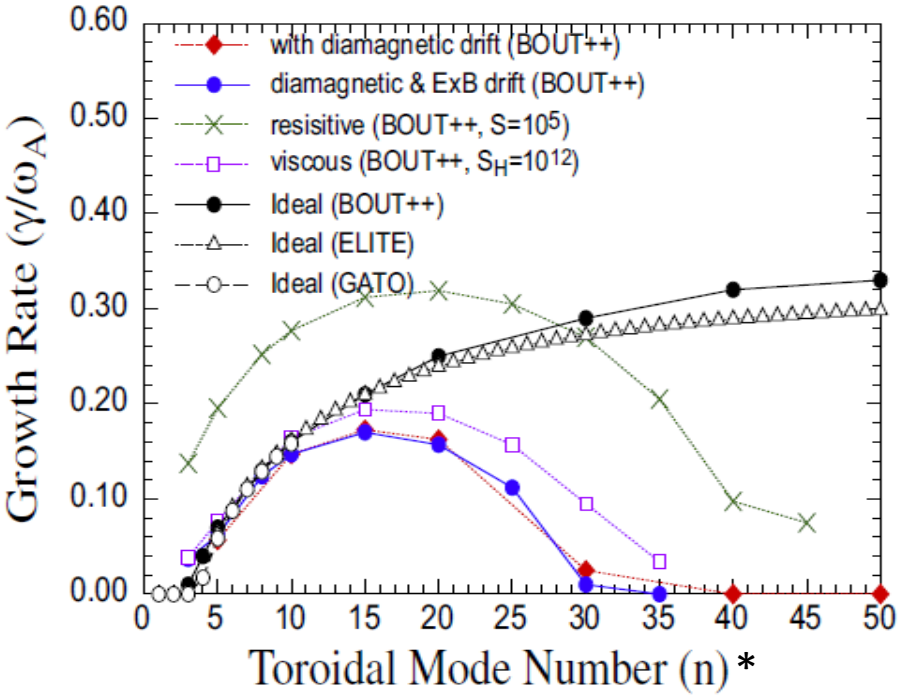

*Xu, X., et al., *Nucl. Fusion* 51 103040 (2011)

Geometry of BOUT++

All the simulations for these work are based on the shift circular cross-section toroidal equilibria (cbm18_dan8) generated by TOQ codes*. The equilibrium pressure is the same for all cases.

- JET-like aspect ratio
- Highly unstable to ballooning modes ($\gamma \sim 0.2\omega_A$)
- Widely used by NIMROD, M3D, M3D-c1

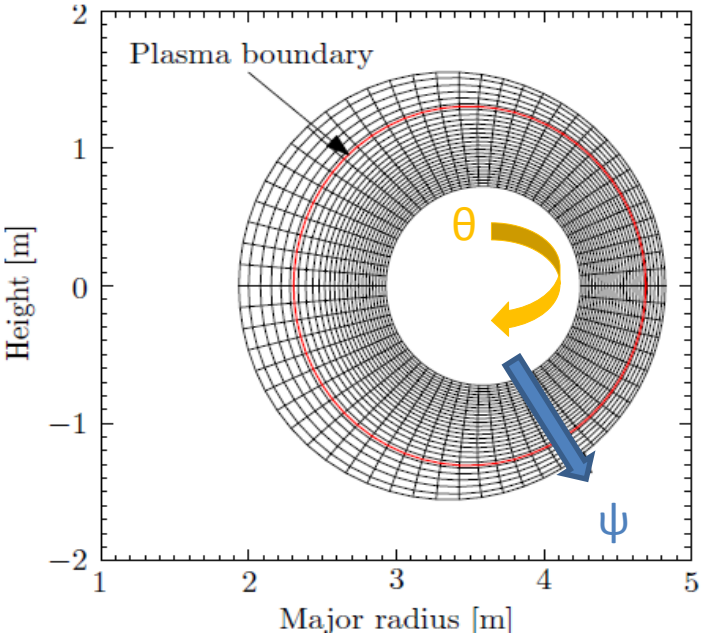

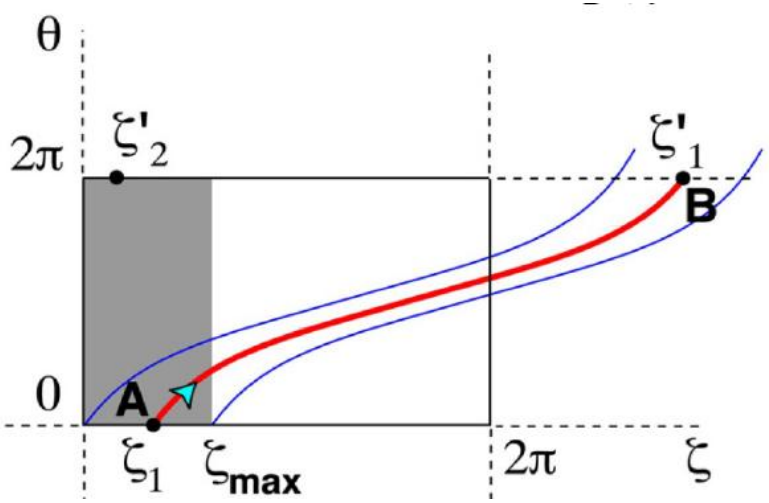

Field aligned coordinate applied in BOUT++:

$$x = \psi - \psi_0,$$

$$y = \theta,$$

$$z = \zeta - \int_{\theta_0}^{\theta} \nu(\psi,\theta)\,d\theta$$

$$\nu(\psi,\theta) = \frac{\vec{B}\cdot\nabla\zeta}{\vec{B}\cdot\nabla\theta}$$

* Miller R.L. and Dam J.W.V. *Nucl. Fusion* 27 2101 (1987).

Theoretic Model for 5-Field in BOUT++

We extend the peeling-ballooning model with non-ideal physics effects to include: diamagnetic drift, ExB drift, resistivity and anomalous electron viscosity. We evolve a set of nonlinear evolution equations for perturbations of the ion number density n_i, ion temperature T_i, electron temperature T_e, vorticity ϖ and magnetic flux ψ:

$$\varpi = n_{i0}\frac{m_i}{B_0}\left[\nabla_\perp^2\phi + \frac{1}{n_{i0}}\nabla_\perp\phi\cdot\nabla_\perp n_{i0} + \frac{1}{n_{i0}Z_i e}\nabla_\perp^2 p\right],$$

$$\frac{\partial P}{\partial t} + \mathbf{V}_E\cdot\nabla P = 0 \quad (previous\ model)$$

$$\frac{\partial n_i}{\partial t} + \mathbf{V}_E\cdot\nabla n_i = 0,$$

$$\frac{\partial T_j}{\partial t} + \mathbf{V}_E\cdot\nabla T_j = 0,$$

$$J_\parallel = J_{\parallel 0} - \frac{1}{\mu_0}\nabla_\perp^2(B_0\psi),$$

$$\mathbf{V}_E = \frac{1}{B_0}(\mathbf{b}_0\times\nabla_\perp\Phi),$$

$$\frac{\partial}{\partial t}\varpi + \mathbf{V}_E\cdot\nabla\varpi = B_0\mathbf{b}\cdot\nabla\frac{J_\parallel}{B_0} + 2\mathbf{b}\times\kappa\cdot\nabla P,$$

$$P = k_B n(T_i + T_e) = P_0 + p,$$

$$\frac{\partial\psi}{\partial t} = -\frac{1}{B_0}\mathbf{b}\cdot\nabla\Phi + \frac{\eta}{\mu_0}\nabla_\perp^2\psi - \frac{\eta_H}{\mu_0}\nabla_\perp^4\psi,$$

$$\Phi = \Phi_0 + \phi.$$

Diamagnetic stabilization on linear growth rate for spatial constant n_0

For Ideal MHD, spatial constant n_0 is equivalent to the previous 3-field results because the density terms do not appear in ideal MHD.

The dispersion relation is written as

$$\omega^2 + \omega \frac{1}{n_{i0} Z_i e} (\mathbf{b}_0 \times \mathbf{k} \cdot \nabla P_0) = \frac{2}{k_\perp^2 n_{i0}} (\mathbf{b}_0 \times \mathbf{k} \cdot \nabla P_0)(\mathbf{b}_0 \times \kappa \cdot \mathbf{k}) + \frac{B_0^2 k_\parallel^2}{n_{i0}} - \frac{B_0^2 k_\parallel (\mathbf{b}_0 \times \mathbf{k} \cdot \nabla J_{\parallel 0})}{n_{i0} k_\perp^2}.$$

$$\frac{\gamma_{nd}^2}{\omega_A^2} = \frac{\gamma_{nc}^2}{\omega_A^2} + i \frac{\gamma_{nd}}{\omega_A} \frac{1}{\sqrt{n_{i0}} Z_i e} (\mathbf{b}_0 \times \mathbf{k} \cdot \nabla P_0)$$

γ_{nc} is the growth rate in ideal MHD and γ_{nd} is the growth rate with diamagnetic effects.

The diamagnetic drift term provides a real frequency and stabilizing effect. So the linear growth rate is proportional to n_0.

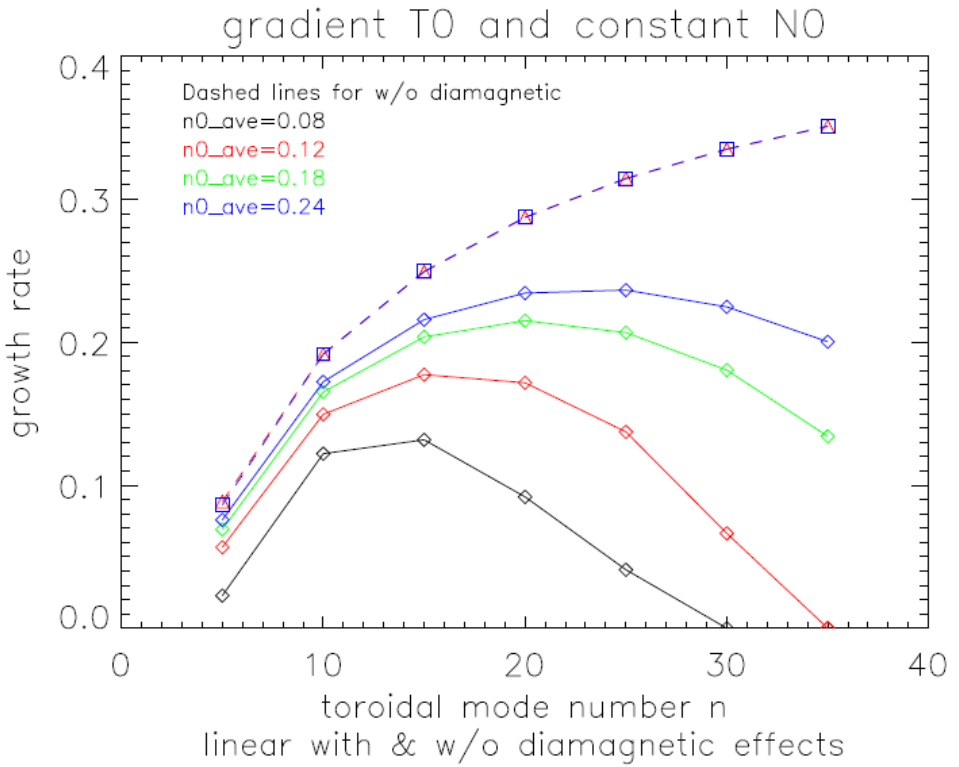

Diamagnetic stabilization on linear growth rate for spatial constant T_0

If T_0 is a spatial constant, then the cross term in the Laplace equation of vorticity generate novel effects.

- For Ideal MHD, the cross term just plays as the oscillatory term, so for this case the linear growth rate should not changed a lot.
- With diamagnetic effects, the linear growth rate is inversely proportional to T_0.

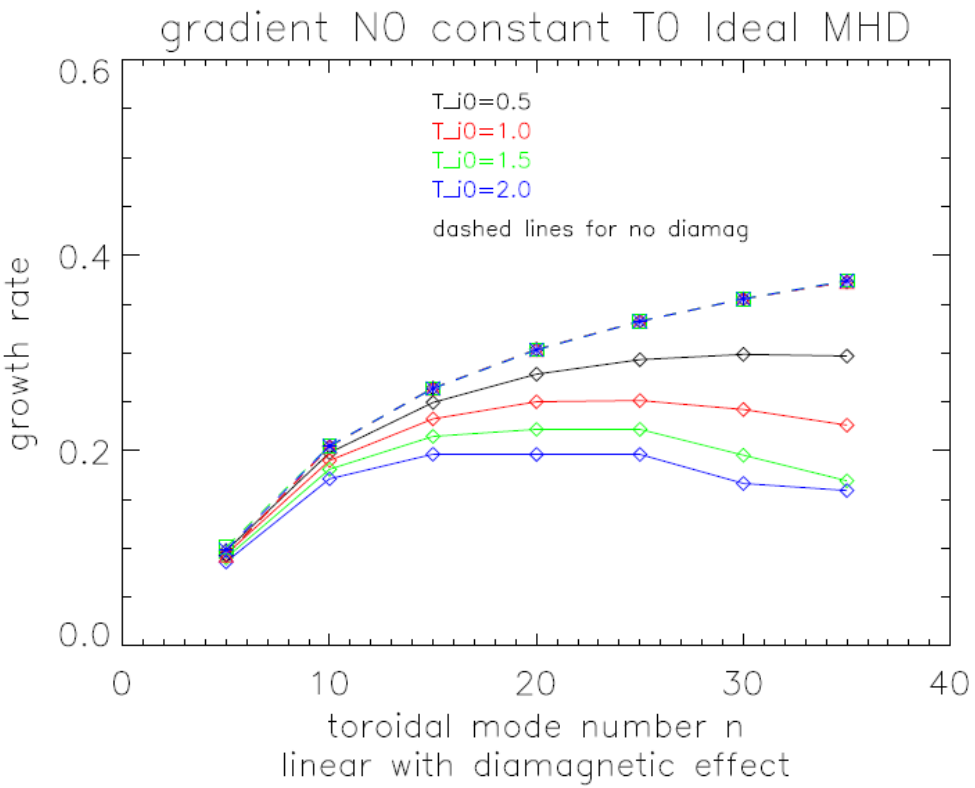

General cases for both radially varying n_0 and T_0

For more general situation, both the equilibrium temperature and density profiles are not constant in radial direction. Here we still apply the same pressure profile, but introduce the profile for ion density:

$$n_{i0}(x) = \frac{(n0_{height} \times n_{ped})}{2}\left[1 - \tanh\left(\frac{x - x_{ped}}{\Delta x_{ped}}\right)\right] + n0_{ave} \times n_{ped},$$

There are 5 density profiles are applied in this work:

	$n0_{ave}$	$n0_{height}$	$n0_{bot}$ $(\times 10^{19})$	$n0_{top}(\times 10^{19})$	$n0_{ped-top}(\times 10^{19})$
Case 0	0.12	0	1.00	1.00	1.00
Case 0'	-	-	0.09	8.97	3.98
Case 1	0.02	0.24	0.24	2.33	1.00
Case 2	0.02	0.30	0.25	2.87	1.29
Case 3	0.02	0.45	0.29	4.22	2.18

Table 1. The parameters of five models of different equilibrium ion density profile.

Diamagnetic stabilization on linear growth rate for both radially varying n_0 and T_0

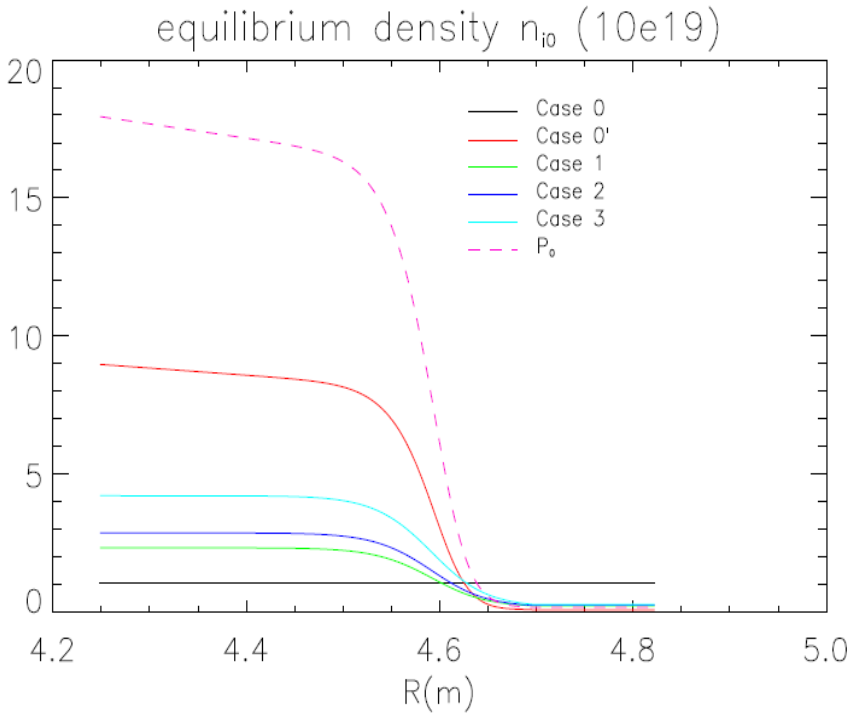

The equilibrium density profiles for the cases in Table 1.

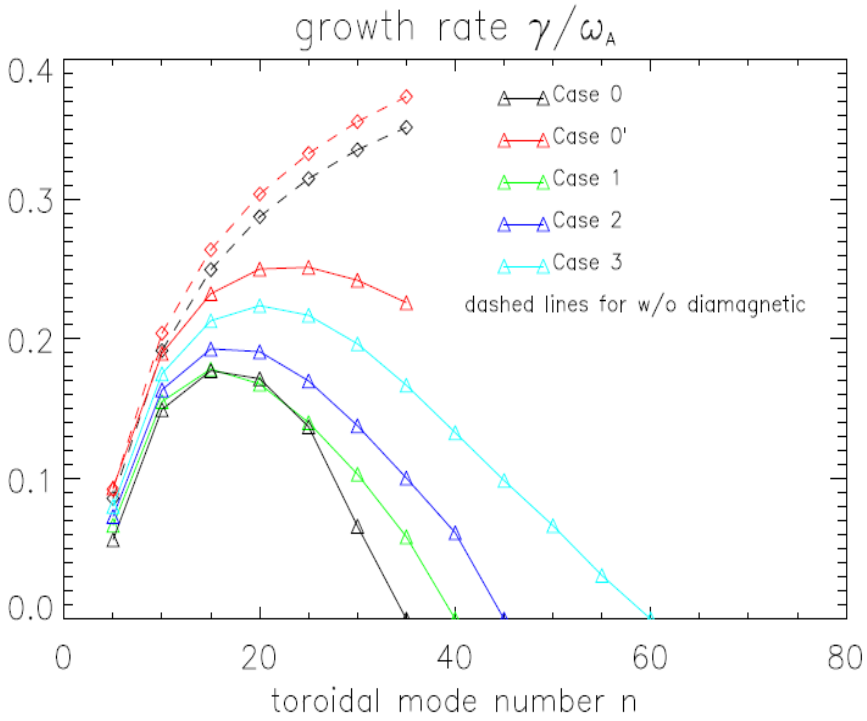

The linear growth rate for the cases in table 1. For Ideal MHD model, the linear growth rate of case 0' is larger than case 0 by 6.2%. With diamagnetic effects, the percentage goes to 31.4% for n=15

The cross term in vorticity can enlarge growth rate

For spatial constant T_0, the Fourier analysis will give the angular frequency as:

$$\begin{aligned}\omega_{Tc}^2 &= \left[\frac{2}{k_\perp^2 n_{i0}}(\mathbf{b}_0\times\mathbf{k}\cdot\nabla P_0)(\mathbf{b}_0\times\kappa\cdot\mathbf{k})\right.\\ &\left.+\frac{B_0^2k_\parallel^2}{n_{i0}}-\frac{B_0^2k_\parallel(\mathbf{b}_0\times\mathbf{k}\cdot\nabla J_{\parallel 0})}{n_{i0}k_\perp^2}\right]\frac{1}{1+i\frac{1}{k_\perp L_n}}\\ &= \frac{1}{1+i\frac{1}{k_\perp L_n}}\omega_{nc}^2.\end{aligned}$$

Cross term

Then the linear growth rate is easily obtained as:

$$\varpi = n_{i0}\frac{m_i}{B_0}\left[\nabla_\perp^2\phi+\frac{1}{n_{i0}}\nabla_\perp\phi\cdot\nabla_\perp n_{i0}+\frac{1}{n_{i0}Z_ie}\nabla_\perp^2 p\right]$$

$$\frac{\gamma_{Tc}}{\omega_A} = \frac{i\omega_{Tc}}{\omega_A}\simeq\frac{\gamma_{nc}}{\omega_A}\left(1+\frac{1}{8k_\perp^2L_n^2}\right).$$

This equation shows the qualitatively same results as our simulations

➢The similar results have been observed using MINERVA code*. (a) is for spatial constant n_0 and (b) for a radially varying n_0.

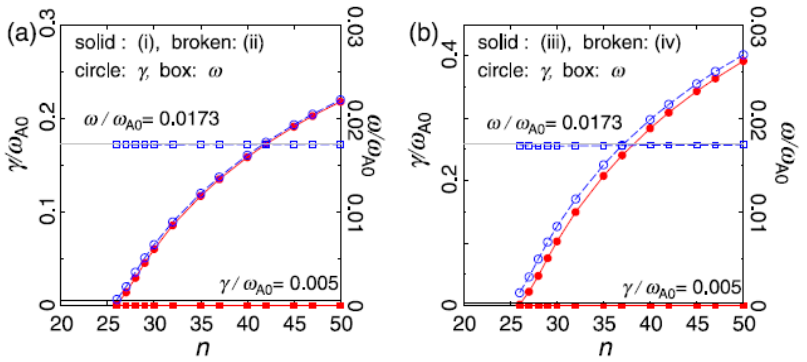

N. Aiba, M. Furukawa, M. Hirota & S. Tokuda, *Nucl. Fusion* 50 045002 (2010) .

Radial pressure profile revolution during ELM crashes

Comparison of the radial pressure profiles on the outer mid-plane for the different cases for n=15.

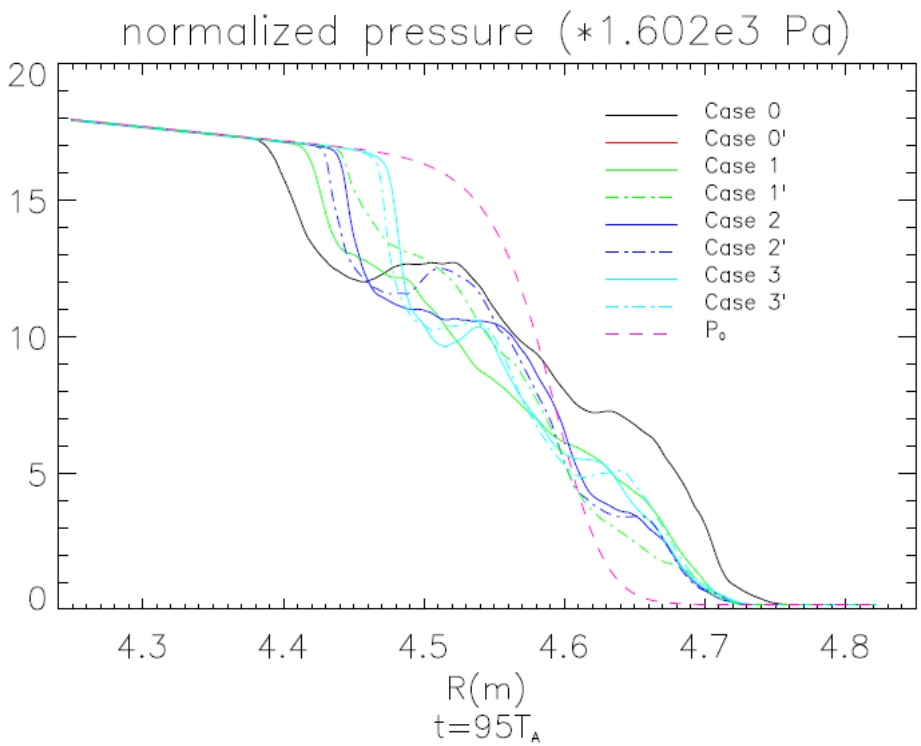

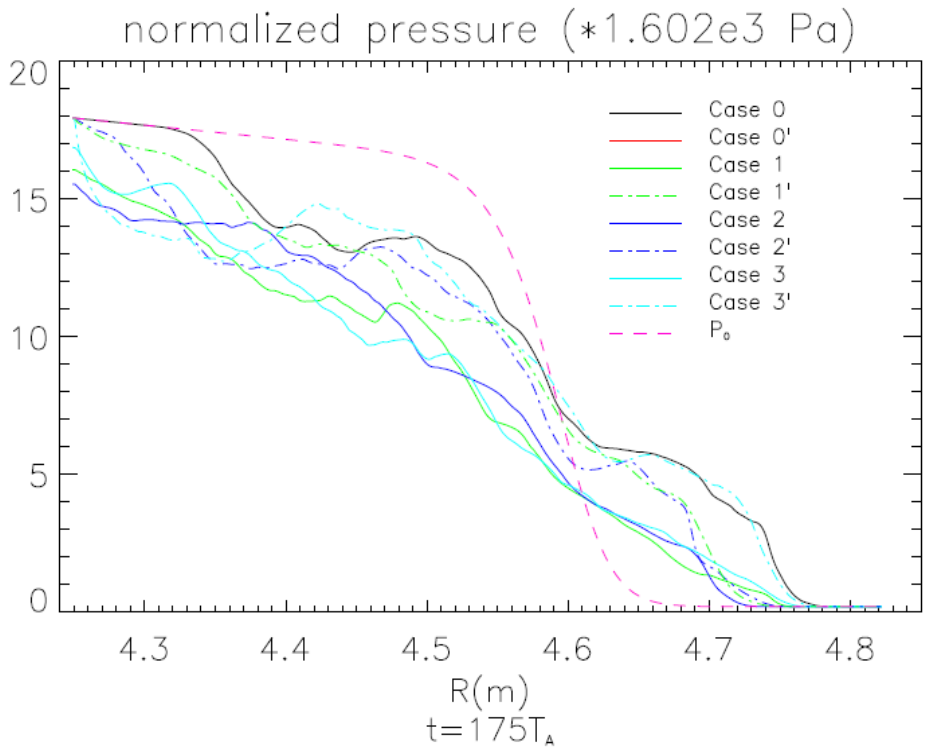

➢Case 1, 2 and 3 use Neumann boundary in the core region and 1', 2' and 3' apply Dirichlet boundary condition.

➢At the early nonlinear phase after ELM crashes, $T=95T_A$, the collapse keeps localized around the peak gradient region for all the cases. The spatial constant n_0 case goes into the core region furthest.

➢When all the cases go into the late nonlinear phase for some time after ELM crashes, $t=175T_A$, the perturbations go into the core boundary except the constant n_0 case. This is because the cross term in the vorticity equation provides an additional drive on the radial direction.

ELM size evolution after ELM crashes

In order to describe the nonlinear effects, we define the ELM size as

$$\Delta_{ELM}^{th} = \frac{\Delta W_{ped}}{W_{ped}} = \frac{\langle \int_{R_{in}}^{R_{out}} \oint dR d\theta (P_0 - \langle P \rangle_\zeta) \rangle_t}{\int_{R_{in}}^{R_{out}} \oint dR d\theta P_0},$$

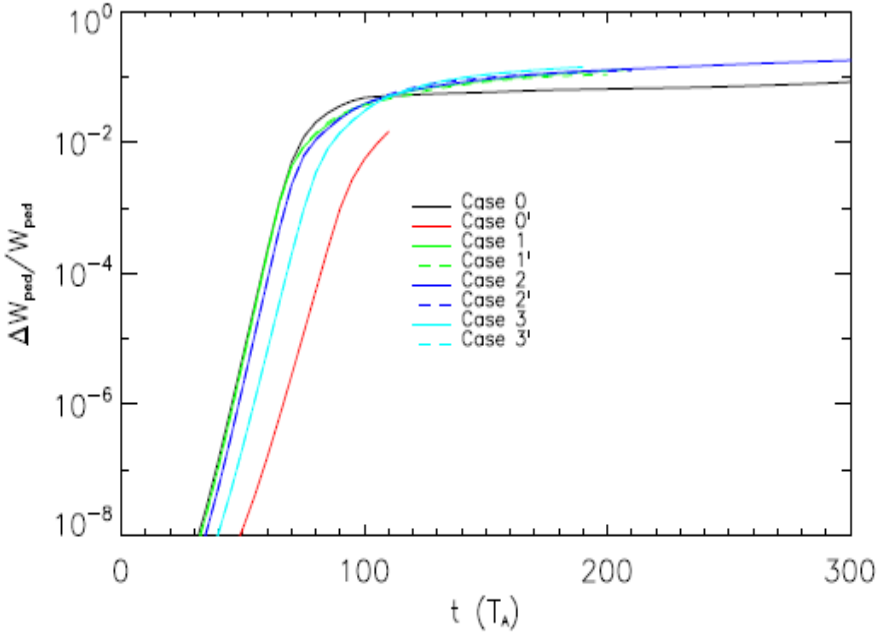

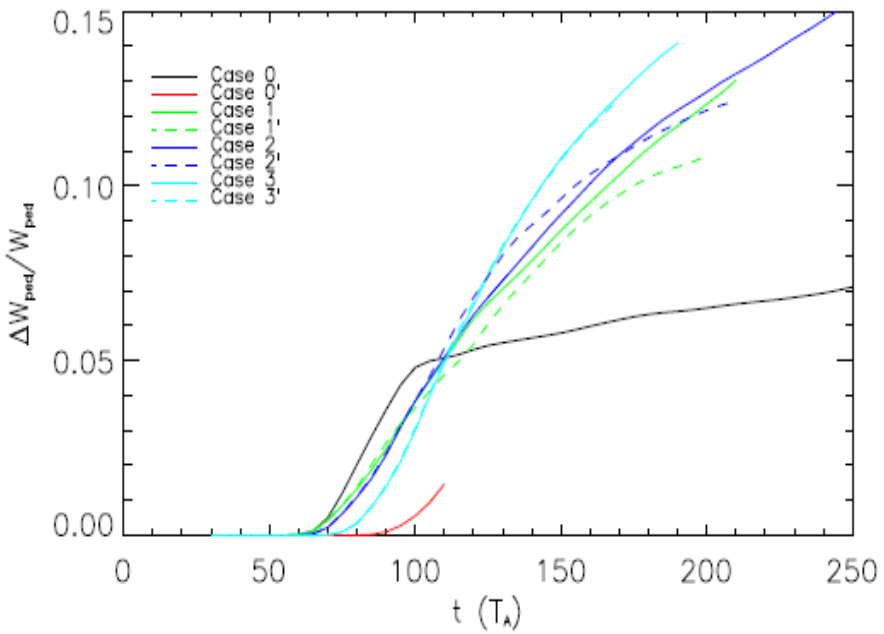

These figures show that the ELM size is larger for a radially varying n_0 than for the spatial constant density case. This is related to the results on the previous page, which showed that the cross term in the vorticity equation provides an additional drive on the radial direction.

The poloidal distribution of pressure perturbation

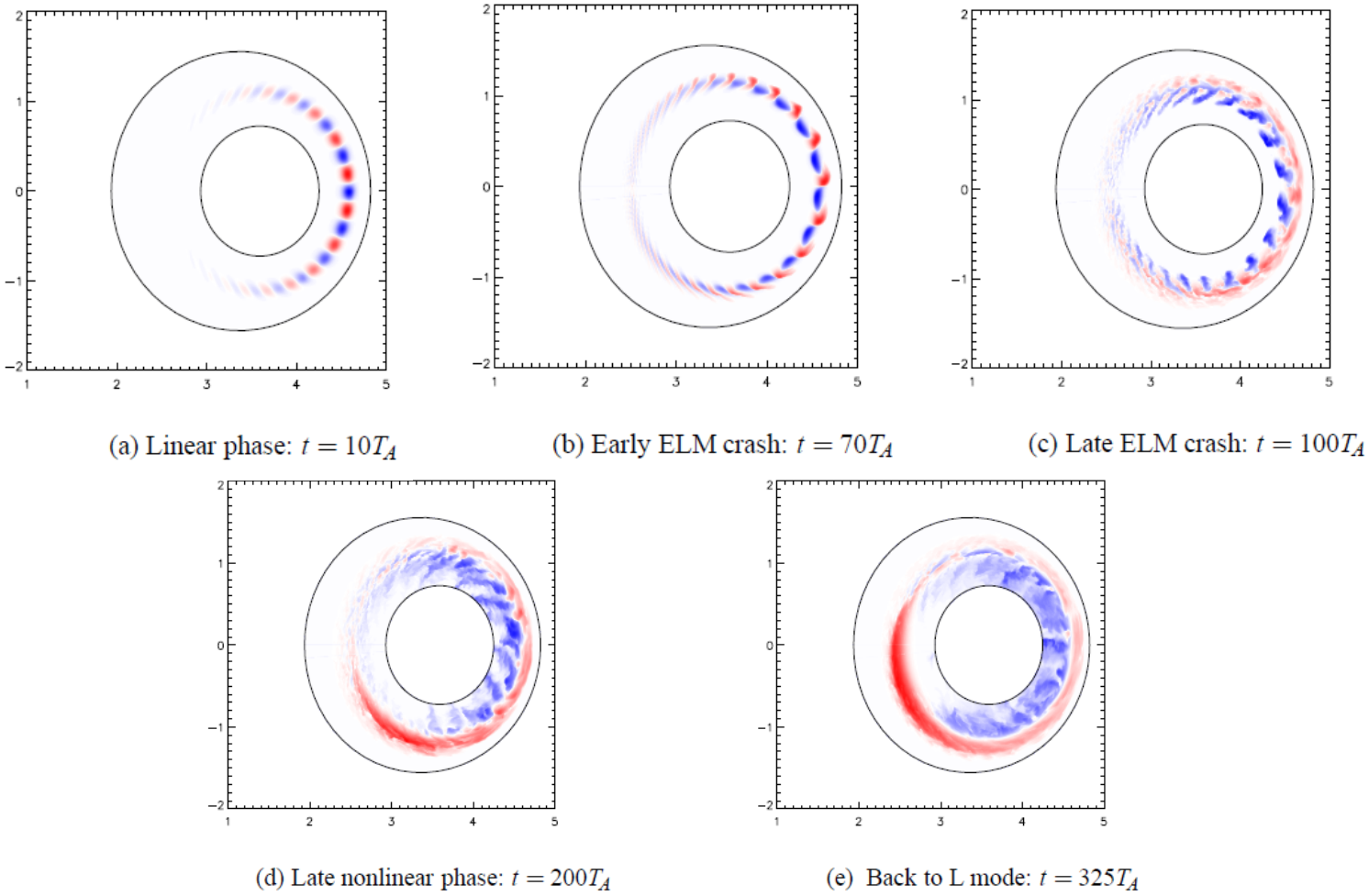

(a) Linear phase: $t = 10T_A$ (b) Early ELM crash: $t = 70T_A$ (c) Late ELM crash: $t = 100T_A$

(d) Late nonlinear phase: $t = 200T_A$ (e) Back to L mode: $t = 325T_A$

Poloidal slices in the shifted circle configuration. The density perturbation at t = $10T_A$, t = $100T_A$, t = $200T_A$ and t = $325T_A$ for Case 2 are shown here. Red colour is for a positive perturbation and blue is for a negative one.

Comparison of differencing schemes for ELM simulations

For the purpose of broad application of BOUT++, various differencing schemes has been implemented. Here we compare the ELM simulations of 3-field model with several differencing methods to find the most robust scheme in ELM simulations.
The schemes used here are all for the nonlinear Poisson bracket. It means the ExB drift $\tilde{V}_E \cdot \nabla$ ($b_0 \times \nabla\Phi \cdot \nabla$) and magnetic flutter $\tilde{b} \cdot \nabla$ ($b_0 \times \nabla\psi \cdot \nabla$). Because the simple methods of straight central or upwinding schemes for both terms will result in the code crashes in the early nonlinear phase, the special schemes are chosen:

- 3rd order WENO: Weighted Essentially Non-Oscillatory, a nonlinear adaptive procedure avoiding crossing discontinuities in the interpolation procedure as much as possible

- Arakawa: second order, keep the commutative property of Poisson bracket, the square vorticity conservation and kinetic energy conservation.

- CTU: Corner Transport Upwind, 1st order, takes into account the effect of information propagating across corners of zones in calculating the flux

- 1st and 4th order Upwind

- 4th order central

Linear growth rates for different schemes are converged to radial resolutions

- All the schemes obtain convergence for sufficiently fine resolution in the radial direction.
- Convergence for the different schemes is expected except for the 1st order upwinding for ExB drift, the reason is under investigation.
- The CTU scheme shows the largest departure from the other schemes in linear growth rate, but the differences are less than 3%.

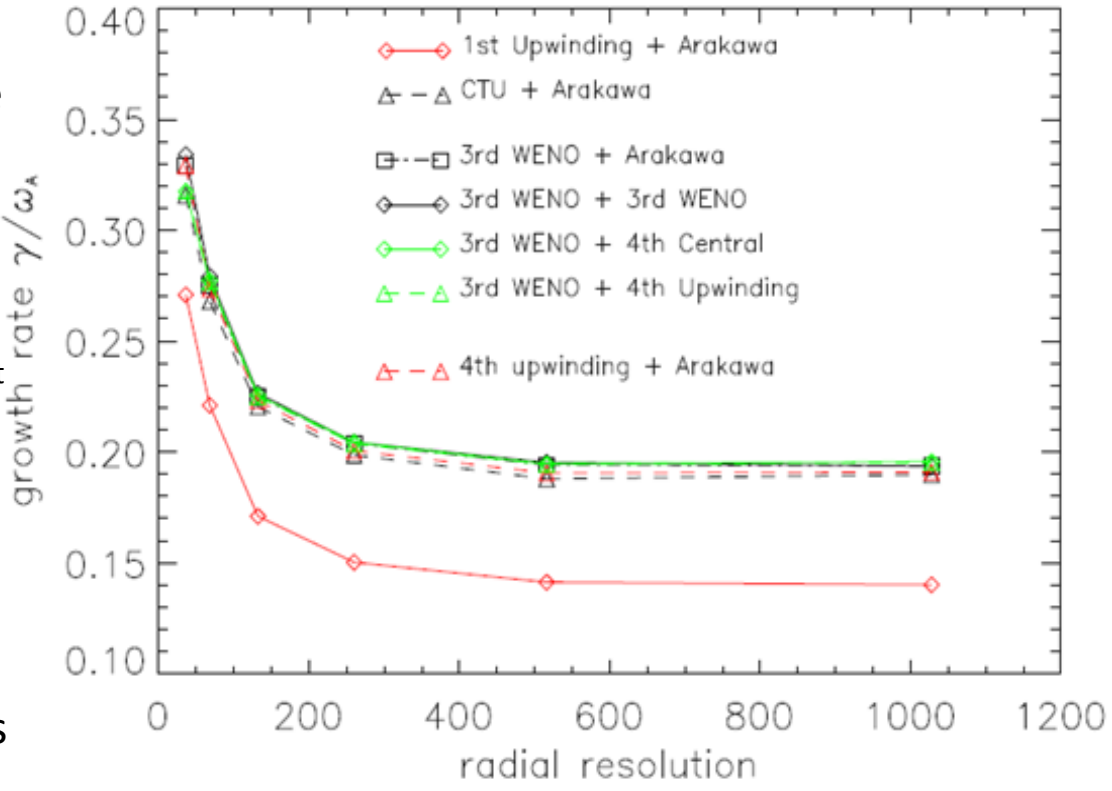

Linear growth rate vs. radial grid resolution.
The schemes are labeled as X+Y:
X is the scheme for ExB drift.
Y is for magnetic flutter term.

Nonlinear: higher order ExB convection schemes yield saturate pressure

- The nonlinear regime shows a more complicated convergence.
- For high resolution, 3rd WENO + 4th order central or + upwinding shows good convergence with 3rd WENO + Arakawa. The difference is less than 3.5%. The full WENO scheme is larger by 15.0%
- The schemes for ExB drift determine the saturate pressure more effectively than $\tilde{b} \cdot \nabla$. Lower order schemes for EXB obtain the lower pressure.

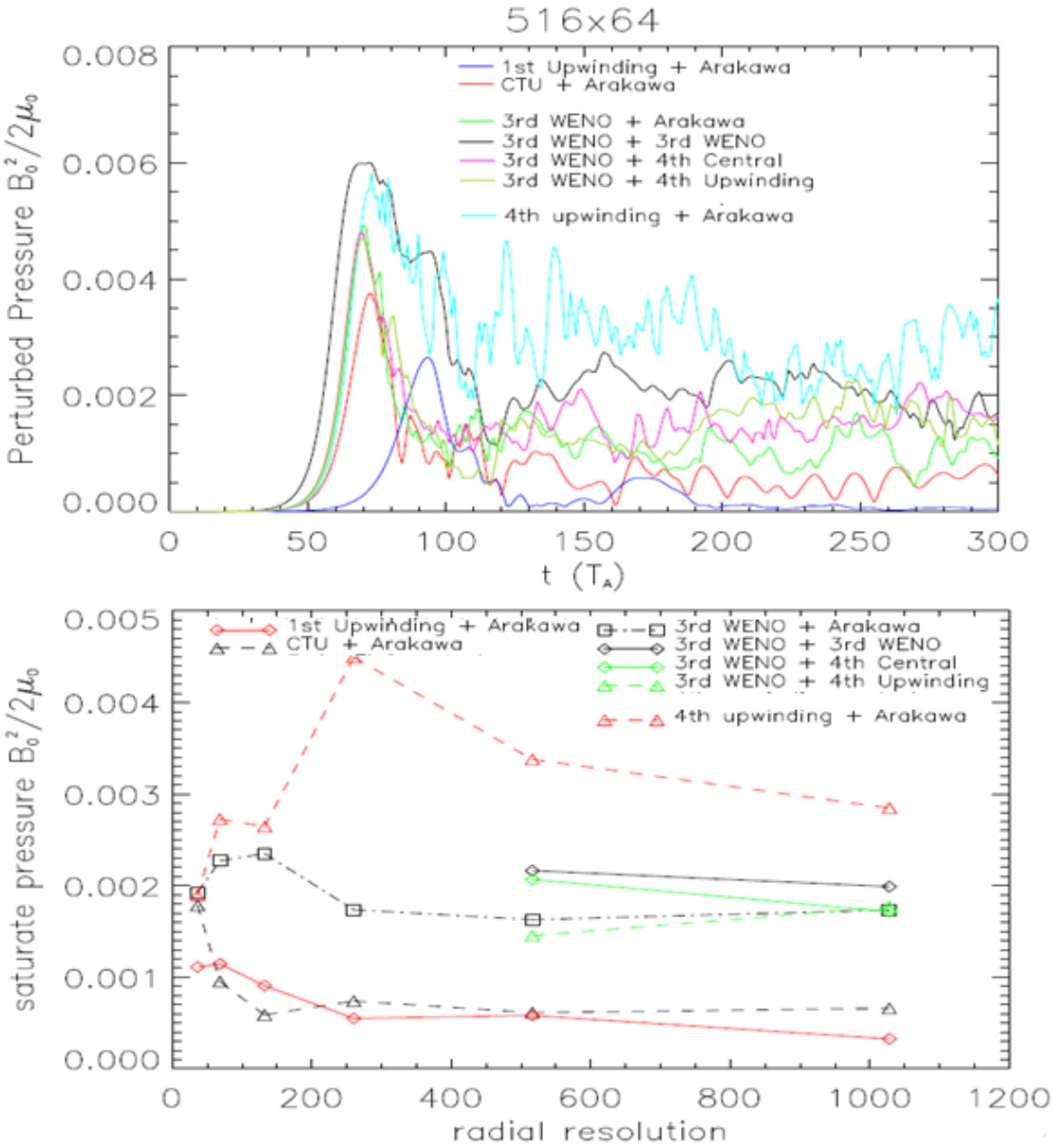

Nonlinear: higher order ExB convection schemes yield ELM size

The ELM size shows the similar conclusion to saturate pressure. Full WENO also shows a very good convergence with the WENO + other schemes, less than 9.5%. At t=140T_A, these scheme combinations with WENO + others differ less than 27.5%, while at t=200T_A the difference is 24.5% in comparison with full WENO.

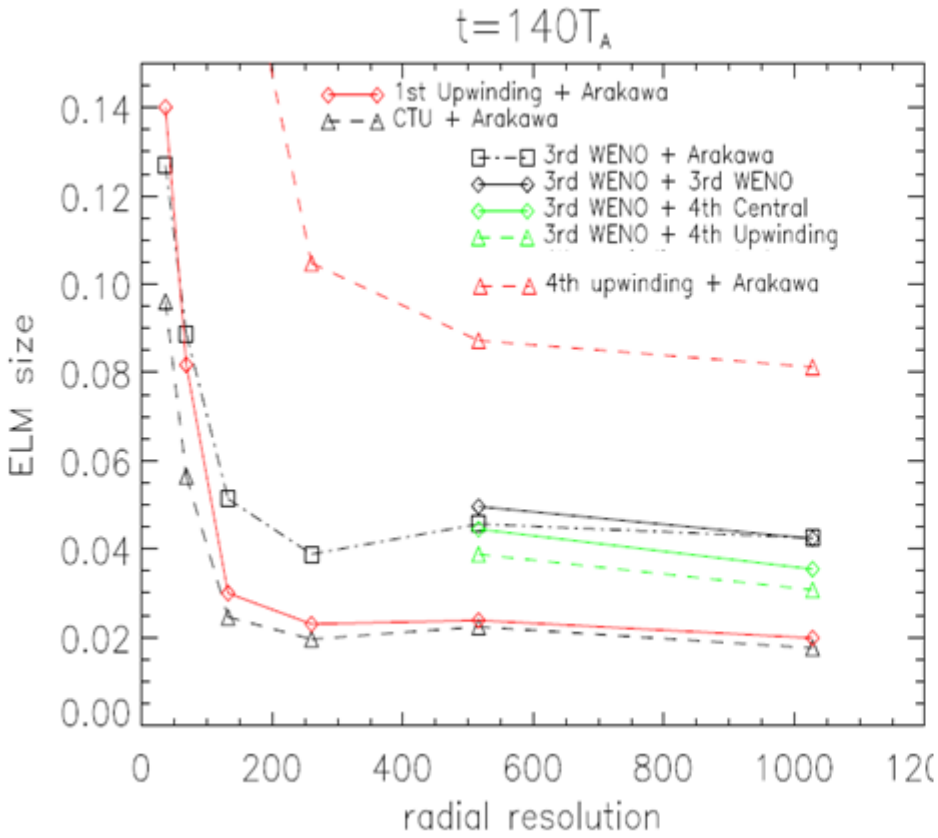

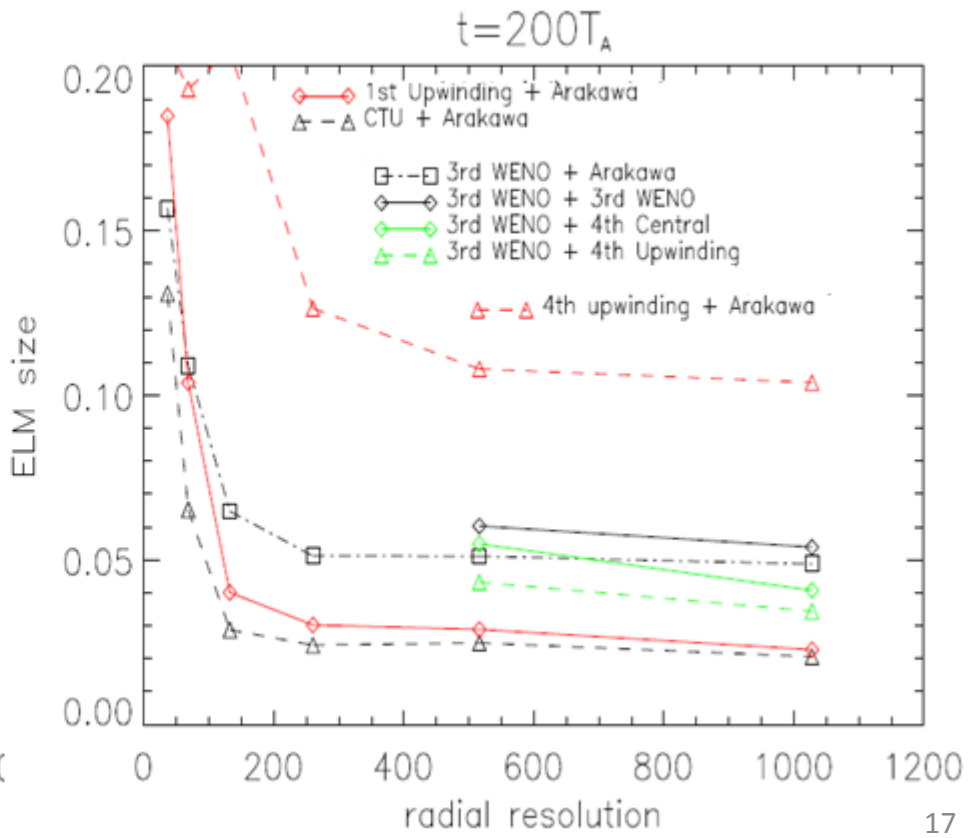

Nonlinear: k_r power spectra of perturbed pressure are converged for $5<k_r<80$

The k_r power spectrum of time averaged radial pressure are shown.

- All the schemes show the similar spectrum at medium k_r: $5<k_r<80$.
- For both resolutions, the 1st upwinding + Arakawa shows to larger spectrum at high k_r.
- For the lower resolution at low k_r position, WENO + Arakawa has the same spectrum as the first order schemes for ExB, which is different from full WENO case. However, at high k_r, these two schemes get almost the same spectrum, which is still much larger than other schemes.
- For the higher resolution case, WENO + Arakawa has the spectrum more close to full WENO. At high k_r end, both spectrums are damped and similar to other schemes.

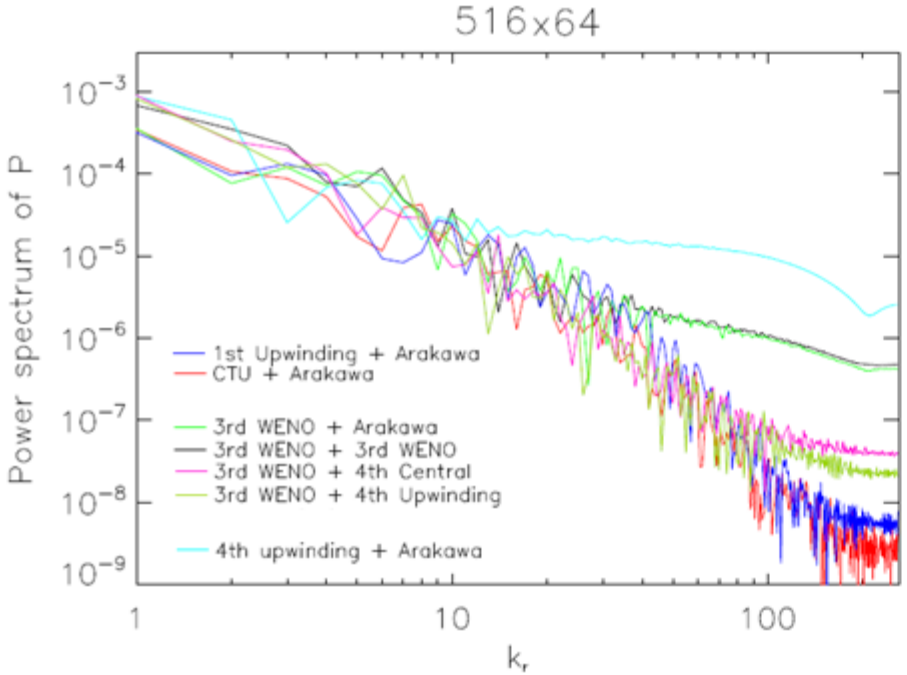

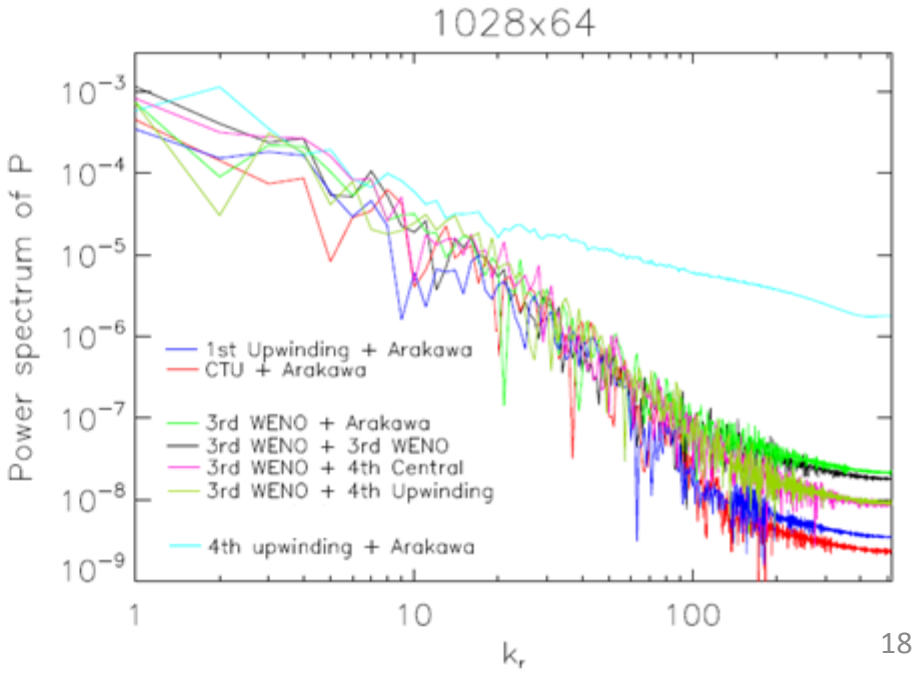

Lower order + Arakawa scheme works well without hyper-resistivity for low radial resolutions

➢In the previous BOUT++ simulations with full WENO schemes, hyper-resistivity η_H is added into the model to prevent the current sheet to become smaller than the grid scale.

➢For the lower resolution grid points, the simulation cannot go through to the ELM crashes except with larger η_H or smaller S_H. For example, we have to use $S_H=10^{11}$ for 260x64 grid and $S_H=1.43\text{x}10^{12}$ for 1028x64 case, while $S_H=1\text{x}10^{12}$ for 516x64.

➢If we change the scheme for magnetic flutter from WENO to Arakawa, the simulation can work well for the resolutions below 1028 even without η_H as the numerical scheme provides enough dissapation. However, η_H is necessary for 1028x64.

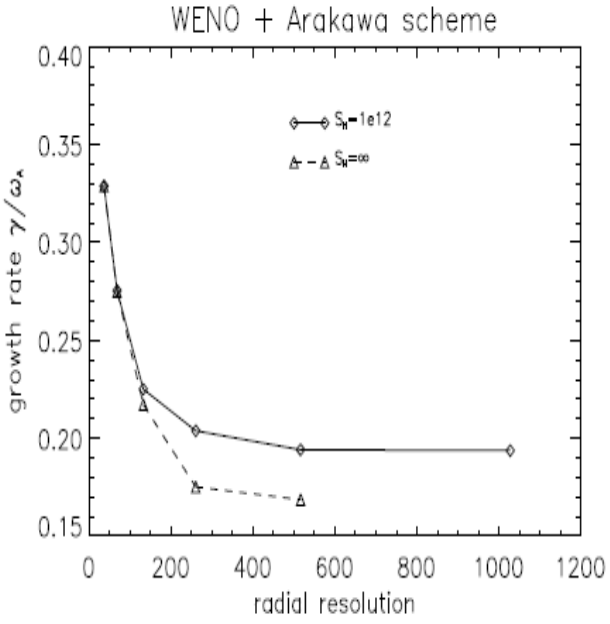

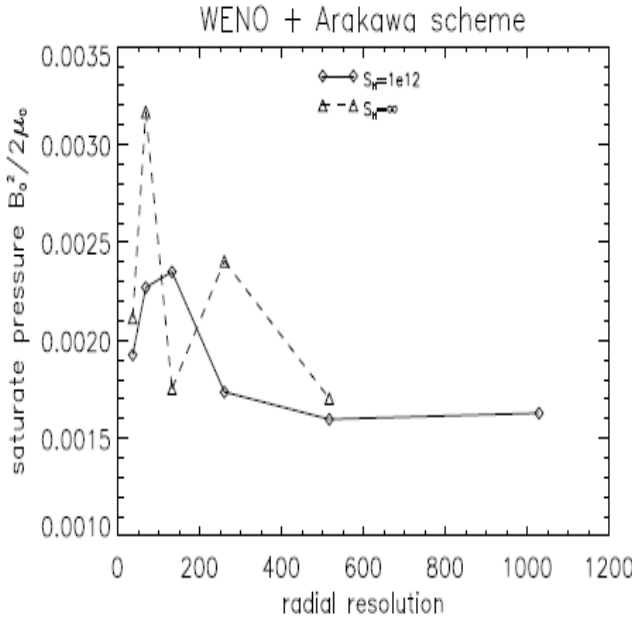

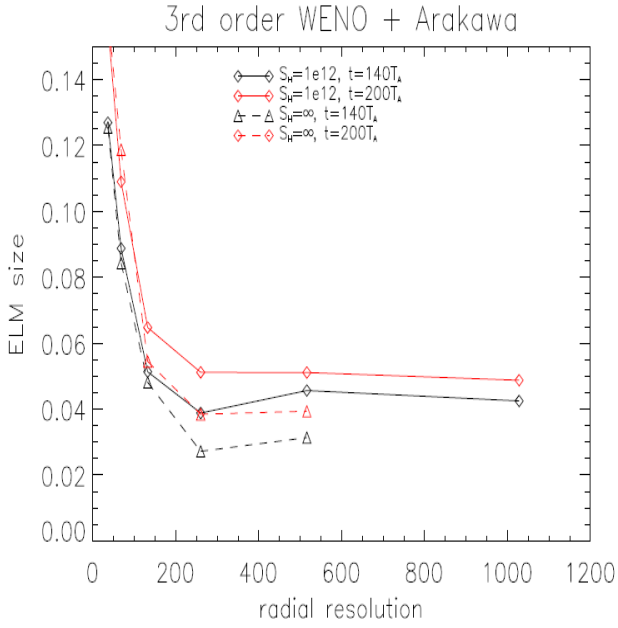

Summary

5-field:

- Introduce the density and temperature into the ELM module of BOUT++ and expand it from 3-field to 5-field model.
- The equilibrium density n_0 will not affect the linear growth rate in Ideal MHD model. With diamagnetic effects, the growth rate is inversely proportional to n_0.
- For the same pressure profile and spatial constant T_0 case, the cross term in vorticity enlarges the growth rate by 6.2% compared with spatial constant n_0 case in Ideal MHD. With diamagnetic effects, the number is 31.4% for n=15.
- The density gradient will drive the perturbation into the core region and give a larger ELM size.

Schemes analysis:

- For linear regime, most of the combinations of the schemes we tested in BOUT++ give the same results.
- For nonlinear regime, the WENO schemes in ExB drift will give more convergent results than other combinations. The Arakawa schemes in nonlinear magnetic flutter help the simulations to go through ELM crashes.
- Lower order schemes yield better convergence with radial resolution scan.
- The k_r power spectrum shows that all the schemes are similar at medium k_r.